Per. Mineral. (2008), 77, 3, 43-64

doi:10.2451/2008PM0018
http://go.to/permin

PERIODICO di MINERALOGIA
established in 1930

An International Journal of
MINERALOGY, CRYSTALLOGRAPHY, GEOCHEMISTRY, ORE DEPOSITS, PETROLOGY, VOLCANOLOGY
and applied topics on *Environment*, *Archaeometry* and *Cultural Heritage*

Mineralogy of inclusions in zircon from high-pressure crustal rocks from the Ulten Zone, Italian Alps

Roberto Braga [1] and Hans-Joachim Massonne [2 *]

[1] Dipartimento di Scienze della Terra e Geologico-Ambientali, Università degli Studi di Bologna, Piazza di Porta San Donato, 1, I-40126 Bologna, Italy
[2] Institut für Mineralogie und Kristallchemie, Universität Stuttgart, Azenbergstr. 18, D-70174 Stuttgart, Germany

Submitted, August *2008 - Accepted,* October *2008*

Abstract. — About 1200 zircons were separated from garnet-kyanite gneiss and migmatites of the Ulten Zone, Italian Alps, representing Variscan lower crust. A cathodoluminescence study reveals zircon with inherited detrital or magmatic cores, a growth mantle of variable thickness and an inclusion-free outermost rim. The most abundant inclusions identified in zircon core and mantle by optical microscopy, back-scattered electron imagery, microprobe analyses and laser-Raman spectroscopy are quartz, potassic white-mica, former melt inclusions and biotite. Less abundant garnet, albite-rich plagioclase, alkali-feldspar, rutile, (Cl-)apatite, monazite, graphite, chlorite, paragonite, staurolite, zoisite/clinozoisite, Ca-amphibole, allanite, magnetite/hematite and pyrite also occur. Generally, the zircon mantle close to the core hosts biotite (Si = 2.58-2.78), potassic white mica (Si = 3.07 – 3.30) and former melt inclusions with SiO_2-rich and peraluminous composition, which is typical for melt produced during the anatexis of a (meta)pelitic source. The calculations of a pressure-temperature pseudosection based on the assumed composition of the sedimentary source of the Ulten Zone crust show that a melt-bearing assemblage including biotite and potassic white mica is stable between 750-800 °C and 8.5-12.5 kbar. These values are interpreted to represent peak metamorphic conditions. Pre-peak conditions were characterized by amphibolite-facies conditions as testified by the presence of paragonite, chlorite and staurolite inclusions in zircon. The lack of diagnostic UHP metamorphic minerals (i.e. coesite, microdiamonds, Na-pyroxene or high-Si phengite) and the omnipresence of biotite indicate that the Ulten Zone lower crust experienced medium- to high-pressure conditions related to crustal thickening (possibly followed by lower crust delamination), without being involved in a deep subduction zone as proposed in earlier works.

Riassunto. — Circa 1200 zirconi sono stati separati da uno gneiss a granato e cianite e da tre migmatiti della Zona d'Ultimo, una porzione di crosta profonda di età Varisica affiorante nelle Alpi Orientali. L'acquisizione di immagini in catodoluminescenza ha permesso di risolvere la struttura interna degli zirconi che consiste in un nucleo ereditato di tipo detritico o magmatico, un mantello di accrescimento e un bordo esterno privo di inclusioni. Le inclusioni negli zirconi sono state identificate per mezzo di microscopia ottica, immagini di elettroni retrodiffusi, analisi in microsonda e microspettroscopia Raman. Nel nucleo e nel mantello dello zircone le inclusioni più abbondanti sono costituite da quarzo, mica bianca potassica, materiale criptocristallino interpretato come ex-inclusioni

* Corresponding author, E-mail: h-j.massonne@imi.uni-stuttgart.de

vetrose e biotite. Altre inclusioni, meno abbondanti, sono rappresentate da granato, plagioclasio albitico, alcali-feldspato, rutilo, (Cl-)apatite, monazite, grafite, clorite, paragonite, staurolite, zoisite/clinozoisite, Ca-anfibolo, allanite, magnetite/ematite e pirite. Di solito il mantello dello zircone, in prossimità del contatto con il nucleo, contiene biotite (Si = 2,58 - 2,78), mica bianca potassica (Si = 3,07 - 3,30) ed ex-inclusioni vetrose ricche in SiO_2 e peralluminose, una composizione tipica dei prodotti anatettici delle (meta) peliti. Il calcolo di un diagramma pressione-temperatura isochimico (pseudosezione) basato sulla composizione del probabile protolite sedimentario delle crosta della Zona d'Ultimo mostra che l'associazione comprendente fuso + biotite + mica bianca potassica è stabile tra 750-800 °C e 8,5-12,5 kbar. Questi risultati sono interpretati come valori di picco metamorfico. Le condizioni pre-picco furono caratterizzate da quelle della facies anfibolitica, come testimoniato dal ritrovamento di paragonite, clorite e staurolite inclusi nello zircone. La mancanza di minerali diagnostici di condizioni UHP come coesite, microdiamante, pirosseno sodico o fengite ricca in Si e la costante presenza di biotite indicano che la crosta profonda della Zona d'Ultimo subì condizioni di medio-alta pressione, collegabili all'ispessimento crostale (probabilmente seguito da delaminazione della crosta profonda), senza essere coinvolta in una zona di subduzione come proposto in precedenti lavori.

Key words: *mineral inclusions, zircon, lower crust, pseudosection, Variscan orogeny, Ulten Zone*

Introduction

It has been well established that zircon is an excellent mineral container because of its robustness under variable pressure and temperature conditions (Chopin and Sobolev, 1995; Sobolev *et al.*, 1991; Tabata *et al.*, 1998). This mineral can, thus, preserve early magmatic and metamorphic minerals even those formed under ultrahigh pressures such as coesite and diamond. Numerous studies on mineral inclusions in zircon (Katayama *et al.*, 2000; Liu *et al.*, 2001; Massonne and Nasdala, 2003; Parkinson and Katayama, 1999; Ye *et al.*, 2000) have added pressure-temperature constraints to the prograde and peak conditions attained by crustal units involved in collisional orogens. The above studies permitted to recognize metamorphic peak events in felsic crustal rocks where the late, pervasive retrogression typically obliterates the early metamorphic record.

In this study, we have investigated mineral inclusions in zircon separated from samples representative of the continental crust of the Variscan Ulten Zone (UZ, Fig. 1) in the Italian Alps. We will provide petrographic and mineral chemistry evidence, supported by thermodynamic calculations of P-T pseudosections, that former melt inclusions, related to peak metamorphic conditions, and specific minerals are preserved in particular zircon domains. Additionally, it is most probable that the metamorphic evolution of the Ulten Zone crust remained in the quartz and biotite stability field where partial melting occurred at lower pressures than previously thought.

Composition of the Ulten Zone crust and previous *P-T* estimates

In the Italian Eastern Alps (Fig. 1), the UZ is part of the Upper Austroalpine domain, a nappe pile of Cretaceous age (Thöni, 1981) consisting of metasedimentary cover and upper-to-lower crust units. North of the Giudicarie Line, the Austroalpine domain comprises the Tonale Nappe formed by the Tonale and Ulten zones. The basement of the Tonale Zone, which is characterized by sillimanite-bearing assemblages in metapelitic rocks, was variably retrogressed during late- or post-Variscan exhumation and locally deformed under greenschist facies conditions during the Alpine orogeny (Thöni, 1981). Conversely, the Variscan basement of the UZ reached high-pressure granulite-facies in the kyanite-bearing metapelitic rocks and was not affected by the Alpine overprint (Godard *et al.*, 1996).

The UZ mainly consists of garnet-kyanite gneisses, migmatites, and minor amphibolites. Very rare retrogressed eclogites (Godard *et al.*, 1996; Hauzenberger *et al.*, 1996) and peridotites (Obata and Morten, 1987) appear as lensoid bodies in the UZ crust. Garnet-kyanite gneisses are strongly foliated with quartz + plagioclase + alkali-feldspar layers alternating with layers rich in biotite-garnet-kyanite-rutile (± white-mica). This structure is interpreted as the result of the transposition of former leucosome and

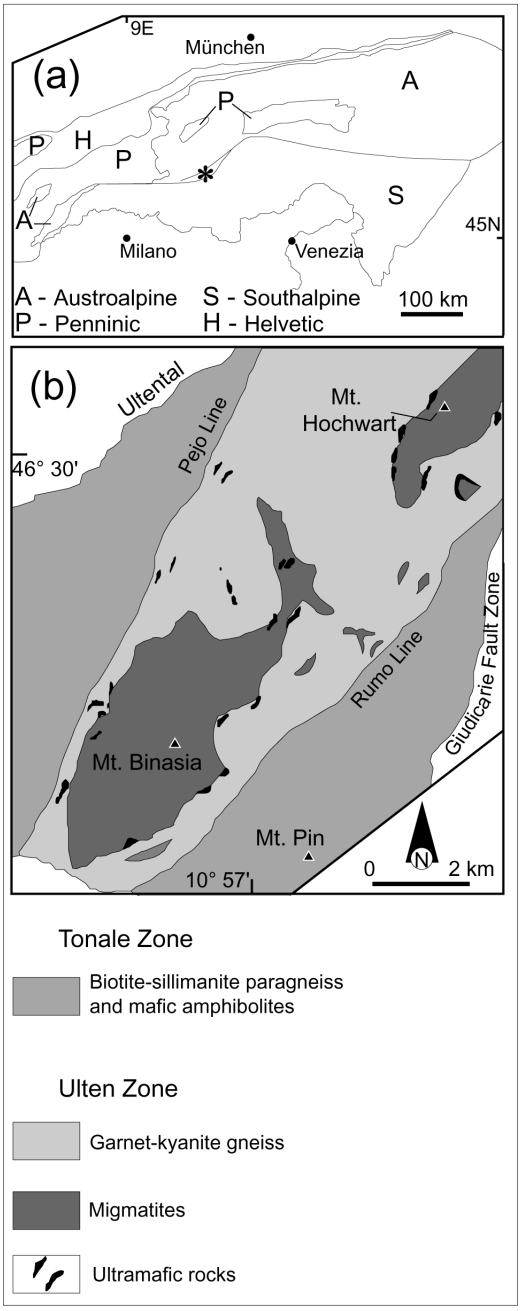

Fig. 1 – (a) Main units of the Alps. The asterisk shows the position of the Tonale Nappe. (b) Simplified geological map of the Ulten Zone (modified from Del Moro *et al.*, 1999).

melanosome along the S1 foliation (Godard *et al.*, 1996). Migmatites range from melanocratic, biotite-rich rocks to leucocratic, plagioclase- and quartz-rich rocks and are interpreted as the product of anatexis of the garnet-kyanite gneisses driven by white-mica dehydration melting (Godard *et al.*, 1996). The peridotites record the transition from spinel- to garnet-facies (Obata and Morten, 1987) and attained peak pressure conditions possibly exceeding 27 kbar and 850 °C (Nimis and Morten, 2000).

The available thermobarometric estimates for the UZ crust (Fig. 2) define a metamorphic evolution characterized by a high-pressure (*HP*) peak followed by retrogression under amphibolite- to greenschist-facies conditions. Using multi-equilibrium geothermobarometry, Godard *et al.* (1996) calculated for the garnet-kyanite gneisses an equilibration range of 10-20 kbar, 600-900 °C. However, migmatites record pressure conditions below 10 kbar. Based on cation exchange and net-transfer geothermobarometry coupled with multi-equilibrium calculations Hauzenberger *et*

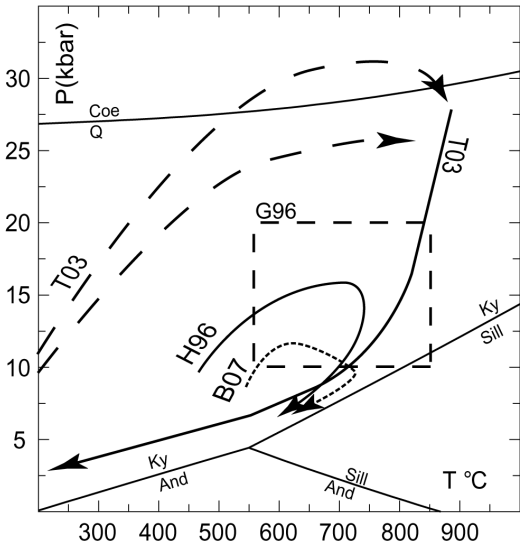

Fig. 2 – **Summary of the** *P-T* estimates for the UZ crust. The curves related to the quartz-coesite transition and the stability of the Al_2SiO_5 polymorphs have been calculated using PERPLE_X and version 5.5 of the Holland and Powell (1998) thermodynamic data set. **G96, Godard** *et al.*, 1996; H96, Hauzenberger *et al.*, 1996; T03, Tumiati *et al.*, 2003; B07, Braga *et al.*, 2007.

al. (1996) suggested a metamorphic peak of at least 15 kbar and 750°C. According to Tumiati *et al.* (2003), the prograde metamorphic evolution of the UZ crust reached a pressure peak near or within the coesite stability field (> 25 kbar) about 330 Ma ago. Mineral inclusions in large kyanite porphyroblasts along with calculated *P-T* pseudosections presented by Braga *et al.* (2007) permitted to reconstruct a *P-T* path characterized by a prograde epidote-amphibole-facies stage, a pressure peak at about 11-12 kbar and a subsequent temperature increase up to ~ 750 °C. The observation, in a single tectonic unit, of *P-T* paths characterized by different peak conditions has been previously made in collisional orogens (e.g., Willner *et al.*, 2000) and may be the result of incomplete (U)HP processing of large (tens of km^2 in size) crustal blocks (Young *et al.*, 2007) or the tectonic assemblage of crustal slivers, suffering very different *P-T* paths, finally amalgamated within a subduction channel (Bousquet, 2008).

The retrograde metamorphic evolution of the UZ crust is thought to be a two-stage process (Ranalli *et al.*, 2005): firstly, a near-isothermal decompression *P-T* path brought a mélange of crustal and mantle rocks to mid-crustal levels (P = 7 kbar and T ~ 500 °C) in late Variscan times (~300 Ma), which were constrained on the basis of Rb-Sr white-mica geochronology (Hauzenberger *et al.*, 1993); secondly, the UZ basement underwent a slow decompression cooling path that ended in Permian-Jurassic times as indicated by Rb-Sr ages of biotite (Del Moro *et al.*, 1993).

Samples and methods

Zircon concentrates were obtained from four samples representative of the UZ crust (see Bargossi *et al.*, 2003, for the sample localities): a garnet-kyanite gneiss (sample NB7), two melanocratic migmatites (NB2 and NB11, the former locally preserving the foliated structure of the source rock) and one plagioclase-rich leucocratic migmatite (NB16).

Zircon concentrates were prepared by sieving about 1 kg of crushed rock to obtain the 0.125-0.0625 mm fraction. This fraction was processed by magnetic and heavy liquid separation techniques to gain zircon concentrates. Finally, zircon grains were hand picked and mounted on an epoxy disk that was attached to the glass-bearer of a standard thin section. The final polishing procedure resulted in the exposure of minerals enclosed in zircon. About 200, 700 and 300 zircon grains were considered for garnet-kyanite gneiss, melanocratic and leucocratic migmatite, respectively. Quantitative chemical analyses from 85 (garnet-kyanite gneiss), 140 (melanocratic migmatite) and 25 (leucocratic migmatite) inclusions were achieved.

Precise quantitative analyses of the inclusion phases were difficult to obtain because of the small area of these phases exposed at the surface. As a consequence, even employing the fully focused beam of an electron microprobe most of the analyses indicated some zirconium (and hence, Si) contamination. The problem was particularly severe for the former melt inclusions that have an average apparent diameter of 2-3 microns. In the case of zirconium contamination, the analysis was recalculated by subtracting ZrO_2 (and the equivalent SiO_2 in a molar ratio ZrO_2:SiO_2 = 1:1) and re-normalized. Therefore, former melt inclusions analyses are considered to be only semiquantitative.

Back-scattered electron (BSE) and cathodoluminescence (CL) images were obtained with specific detectors integrated within a CAMECA SX100 electron microprobe (EMP) installed at the Institut für Mineralogie und Kristallchemie (Universität Stuttgart). Mineral analyses were performed with this EMP equipped with five wavelength dispersive spectrometers. Analyzed elements were Na, Mg, Al, Si, K, Ca, Ti, Mn, Fe and Zr. The latter element was included in the analytical protocol to monitor the possible Zr contamination, caused by the zircon host, of the analytical target. Counting times per element were 20 s at the peak and the background. We used synthetic and natural minerals and pure oxides as standards. Acceleration voltage and primary electric current were 15 kV and 10 nA respectively. A fully focused beam was used. For comparison, ordinary minerals in thin-sections of the rock samples were analyzed as well. For that, conditions were similar with the exception of the beam diameter that was defocused to 5 µm. All raw data were processed with the PaP correction method.

Raman spectra of SiO_2 inclusions were collected with a Jasco NRS 2000 micro Raman at the

Department of Chemistry (Università di Bologna). The instrument was equipped with a 488 nm Kr-Ar laser (Coherent Radiation, Inova 70) with a power of 10 mW. The focused laser beam had a nominal diameter of 1 μm. The spectra were collected from 1100 to 150 cm^{-1} with a resolution of 5 cm^{-1}.

Zircon zonation and petrography of inclusions

Zircon is generally pinkish with ovoid shape; grains with euhedral and faceted external form are very rare. Plain polarized light, CL and BSE images (Figs. 3 and 5) revealed a variety of inclusions, internal structures and luminescence intensity. However, a general pattern can be recognized: an inherited core (c), a mantle (m) and an outermost rim (r) (Fig. 3a). Zircon grains from the garnet-kyanite gneiss show cores with euhedral to anhedral and/or corroded shapes. The internal structures of the cores may show well-developed oscillatory zoning or chaotic structures; the zircon mantle is narrow (or absent) and the rim is structureless with, generally, high luminescence. Zircon grains from the two types of migmatite have either euhedral cores, generally displaying oscillatory zoning, or anhedral/corroded cores with chaotic structures. These grains show a large mantle with oscillatory (zircon from migmatites) or sectoral zoning (zircon from leucocratic migmatite). The outermost rim is structureless and shows either low (zircon from melanocratic migmatite) or high (zircon from leucocratic migmatite) cathodoluminescence.

Single- or multiphase inclusions are located within the zircon core and mantle whereas the outermost rim is inclusion-free (Figs. 3 and 5). The apparent diameter of most of these inclusions varies between 1-5 μm. Only a few inclusions reach larger diameters up to 20 μm. The observed inclusion minerals are listed in Table 1. An SiO_2-phase and micas generally occur in both zircon domains (Fig. 3a-c-d) as well as garnet, which has not been observed in zircon from the leucocratic migmatite. Inclusions with a single Si peak in the energy-dispersive (ED) spectrum are invariably quartz as recognized by micro-Raman spectrometry (Fig. 4). Quartz is generally associated in composite inclusions with biotite (occasionally Ti-rich as indicated by ED spectra) and potassic white-mica. The latter may occur in bimineralic inclusions together with paragonite (Fig. 3e-f). Plagioclase, rare alkali-feldspar, apatite (locally Cl-bearing), and monazite have been found especially in zircon cores. Chlorite, staurolite, allanite, zoisite/clinozoisite, magnetite/hematite and pyrite have been detected only in the zircon core and were not observed in the rock matrix. Rare inclusions of graphite (in melanocratic migmatite NB2, Fig. 5a-b) and Ca-amphibole (in leucocratic migmatite NB16) also occur. Kyanite, which is a major mineral component of the rock matrix, has never been found included in zircon.

At the contact between zircon core and mantle (Fig. 5c-d-e), or in zircon cores with planar oscillatory zoning (Fig. 5f), a common type of inclusion has rounded shape and a few of them may locally form arrays. High-magnification BSE images show that the interior of these inclusions is homogeneous, even though the high illumination of the host zircon may hide internal features. These inclusions are characterized by an ED spectrum with evident peaks of Si, Al, Na and K. For these structural and chemical peculiarities, we interpret these inclusions as cryptocrystalline material representing former melt inclusions.

Chemical composition of inclusion phases

Former melt inclusions are SiO_2-rich (> 70 wt%) and peraluminous [molar $Al_2O_3/(CaO+Na_2O+K_2O)$ > 1.1], with only one inclusion showing a metaluminous signature (Table 2). The sum of total $FeO + MgO + TiO_2$, which are oxides that do hardly enter the melt during (partial) incipient melting of metasediments (Patiño Douce, 1999), is less than 1.8 wt.%. The composition range of the former melt inclusions is close to the melt obtained from kyanite-zone metapelitic rocks of the Himalayan Main Central Thrust by Patiño Douce and Harris (1998) in experiments at 6-10 kbar, 700-900°C and 0-4 wt% added water.

Tables 3-5 report the analyses of enclosed garnet, white-mica and biotite with limited contamination (ZrO_2 < 0.75 wt%) by the zircon host. *Garnet* within zircon core (garnet-kyanite gneiss sample NB7) has higher X_{Fe} [= atomic $Fe^{2+}/(Fe^{2+}+Mg)$] = 0.75-0.76 and almandine content (X_{Alm} = 0.66-0.67) than garnet in the zircon mantle (X_{Fe} = 0.71; X_{Alm} =

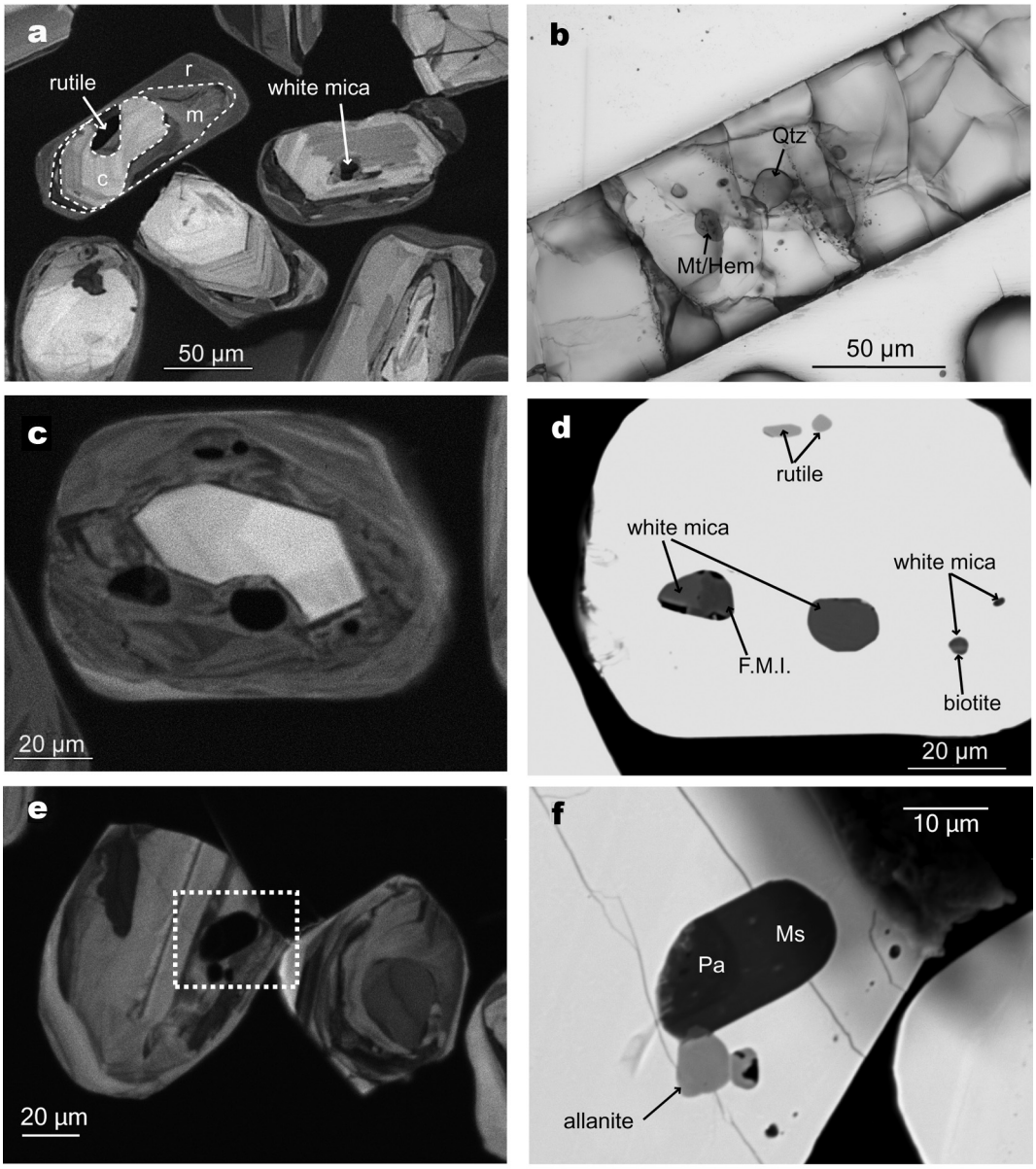

Fig. 3 – Photomicrographs showing the internal structures of zircon grains and type of inclusions. (a) CL image of zircon grains separated from melanocratic migmatite illustrating the different zircon domains; *c*, *m*, and *r* refer to core, mantle and rim, respectively. (b) Plane polarized transmitted light image of a large zircon from the garnet-kyanite gneiss with rounded quartz and hematite/magnetite inclusions. (c-d) CL and BSE images of the same rounded zircon grain; the CL image shows a high-luminescence subhedral core and a low-luminescence mantle with chaotic structures hosting several types of inclusions. (e) CL image of a fragment of zircon from the garnet-kyanite gneiss with a large inclusion; the dotted line refers to image F. (f) BSE image revealing a composite inclusion composed of paragonite + potassic white-mica.

TABLE 1
Minerals included in zircon, garnet and matrix

Sample and rock type	Qtz	Wm	Bt	Grt	Pl	Kfs	Ky	FMI	Rt	Ap	Mnz	C	Chl	Pa	St	Zo Czo	Ca-Amp	All	Mt Hem	Py
NB7 Grt-Ky-gneiss																				
zircon core	•	•	•	•	•	•		•		•	•		•	•		•		•	•	•
zircon mantle		•	•	•																
inclusion in garnet	•	•	•		•	•	•		•											
matrix	•	•	•	•	•	•	•		•	•	•	•								
NB2 Melanocratic migmatite																				
zircon core		•	•	•	•	•		•		•	•				•					•
zircon mantle	•	•	•	•				•	•			•								
inclusion in garnet	•	•	•		•	•	•		•											
matrix	•	•	•	•	•	•	•		•	•	•	•								
NB11 Melanocratic migmatite																				
zircon core	•	•	•		•	•			•	•	•		•							
zircon mantle	•	•	•	•				•	•											
inclusion in garnet	•	•	•		•	•	•		•											
matrix	•	•	•	•	•	•	•		•	•	•	•								
NB16 Leucocratic migmatite																				
zircon core	•	•	•		•			•		•	•		•							
zircon mantle	•	•	•		•	•		•	•								•			
matrix	•	•	•	•	•	•														

Mineral abbreviations: All, allanite; Ap, apatite; Bt, biotite; C, graphite; Ca-Amp, calcic amphibole; Chl, chlorite; Czo, clinozoisite; FMI, former melt inclusion; Grt, garnet; Kfs, alkali-feldspar; Ky, kyanite; Mt/Hem, magnetite/hematite; Mnz, monazite; Pa, paragonite; Pl, plagioclase; Py, pyrite; Qtz, quartz; Rt, rutile; St, staurolite; Wm, potassic white mica; Zo, zoisite.

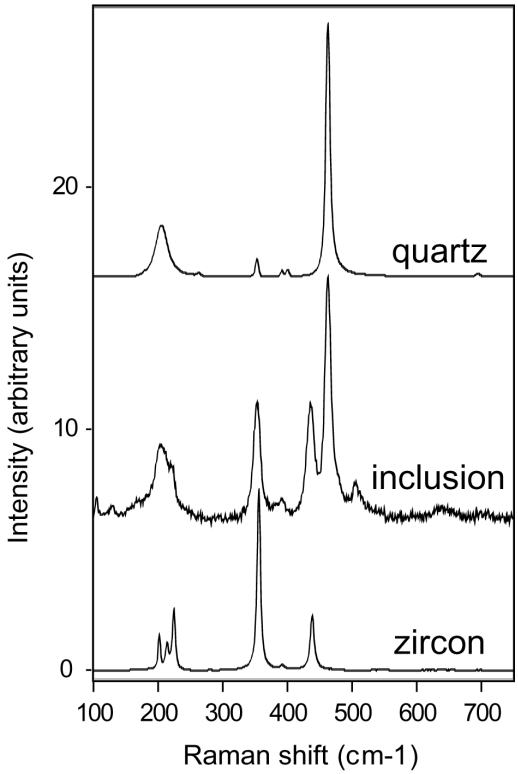

Fig. 4 – Representative Raman spectrum of a quartz inclusion in zircon separated from the garnet-kyanite gneiss. This spectrum contains peaks from the host zircon (see reference spectra).

0.63) with overall limited compositional variation of grossular (X_{Grs}=0.09-0.10) and negligible spessartine content (X_{Sps}=0.01-0.02). The X_{Fe} values (0.71-0.76) are within the X_{Fe} range defined by mm-sized garnet from the rock matrix (Braga *et al.*, 2007). Garnet enclosed in the mantle of zircon from melanocratic migmatite samples NB2 and NB11 is characterized by considerable compositional variation. The range of the X_{Fe} values is 0.71-0.86 and the almandine and pyrope proportions are 0.62-0.75 and 0.12-0.26, respectively. Large variations are also observable in the grossular (0.05-0.12) and spessartine (0.01-0.08) contents. On the other hand, no variations are observed within a single grain, as exemplified by included garnet analyses no. 64-65-66 (Table 3). The comparison between the chemical composition of the included garnet from melanocratic migmatites with the core-rim compositional variation observed in cm-sized matrix garnet from the same rocks (Fig. 6) shows that the latter garnet is characterized by smaller compositional variation than the included garnet. Furthermore, the matrix garnet has X_{Fe} and pyrope and spessartine proportions within the range defined by included garnet. Conversely, matrix garnet has distinctly higher almandine and lower grossular proportions than the included garnet.

White-mica included in core and mantle of zircons from the garnet-kyanite gneiss and the migmatites does not show distinct composition from each other (Fig. 7a). As a whole, the X_{Fe} and Si per double formula unit of potassic white-mica vary from 0.21 to 0.41 and 6.13 to 6.43, respectively. These Si values are intermediate between the average Si contents of matrix white-mica from the garnet-kyanite gneiss and the melanocratic migmatites. The compositional differences between matrix white-mica of the two rock-types reflect different equilibration pressure. In addition, the difference between matrix and included white-mica suggests that the latter was enclosed in zircon during different metamorphic stage(s) compared to the matrix stages of gneiss and migmatite.

White-mica within the core of zircon separated from the leucocratic migmatite forms a distinct group with higher X_{Fe} (0.49-0.54) but similar Si (6.13-6.32) compared to the aforementioned white-mica inclusions. Only two white-micas have been detected in the mantle of zircon separated from the leucocratic migmatite NB16. One of the analyses (not reported in Fig. 7a) resulted in a low K/(K+Na) of 0.78, suggesting that the inclusion is likely a bi-phase inclusion of potassic white-mica and paragonite. This type of multiphase inclusion has been already described by Braga *et al.* (2007) within cm-sized kyanite from a garnet-kyanite gneiss. The only white-mica plotted in Fig. 7a has the highest Si content (6.60 a.p.f.u.) detected among included and matrix white-mica analyzed in this study.

A *biotite* included within the core of zircon from garnet-kyanite gneiss shows significantly higher X_{Fe} (0.55) and lower Si (2.65 apfu) than two biotites included in the zircon mantle (Fig. 7b). Matrix biotite from the same rock-type shows distinctly lower X_{Fe} (0.27) than the biotite in the

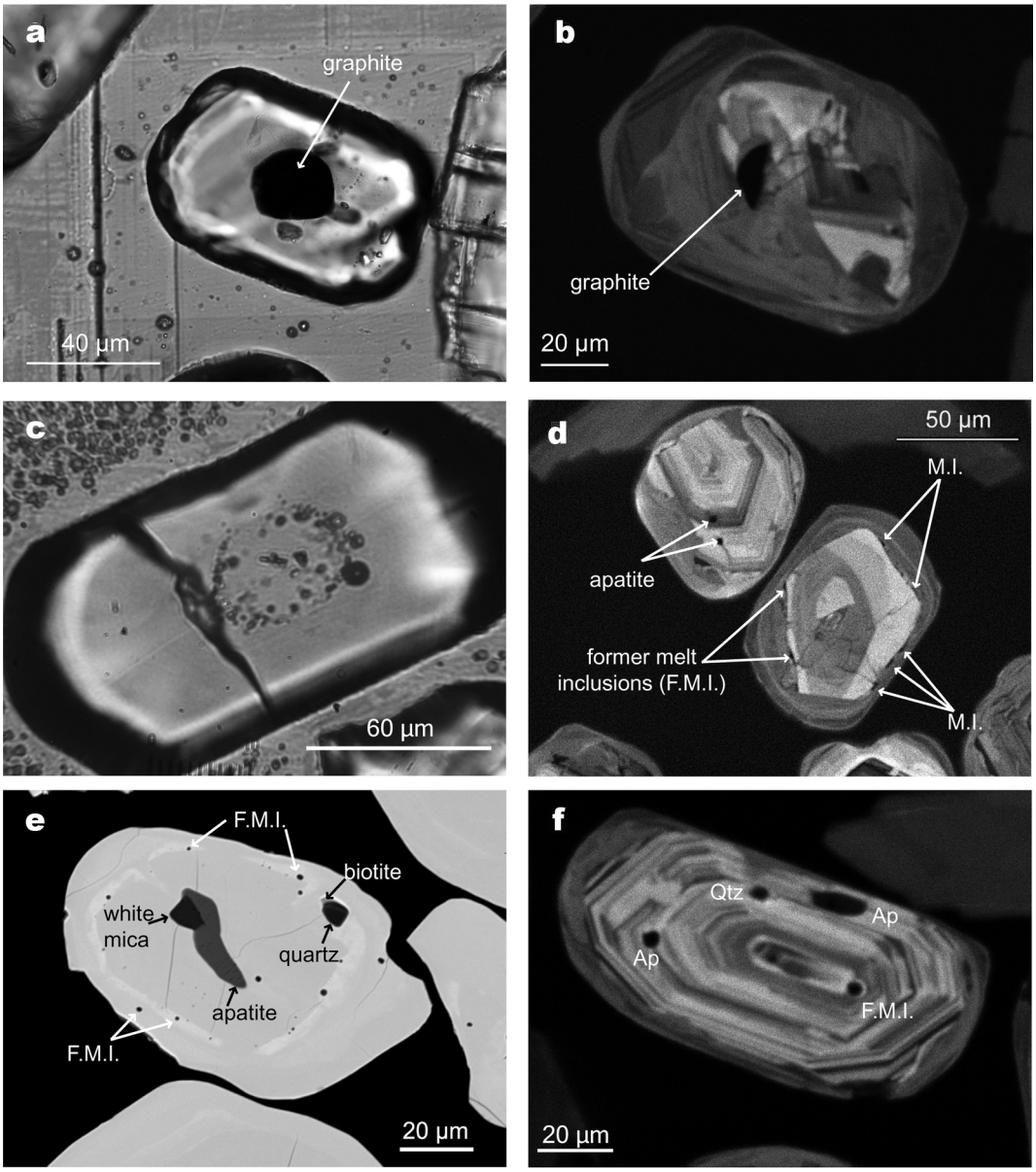

Fig. 5 – (a-b) Optical and CL image of graphite included in the zircon mantle from the melanocratic migmatite NB2; the rounded graphite visible in (a) emerges only partially on the polished surface. (c) Plane polarized transmitted light of a zircon grain with several inclusions of former melt. (d) BSE image showing the distribution of inclusions of former melt (F.M.I) relative to the internal structure of zircon. (e) BSE image of a zircon grain from the melanocratic migmatite: a composite inclusion consisting of apatite + white-mica is located within a zircon core. Inclusions of former melt with rounded shape and a multiphase inclusion of quartz + biotite occur in a narrow zone with high BSE emission; this zone outlines the interface between the zircon core and mantle. (f) Inclusions in a zircon core characterized by planar oscillatory zoning.

TABLE 3
Composition of garnet included in zircon

Sample	NB7 (Grt-Ky-Gneiss)					NB2, NB11 (Melanocratic migmatite)					
ID	#107	#108	#109	#17	#18	#33	#34	#35	#67	#68	#36
Zircon domain	core	core	core	mantle	mantle	mantle	mantle	mantle	mantle	mantle	mantle
SiO_2	37.05	37.19	37.20	37.33	38.12	37.68	37.95	38.10	37.32	37.81	37.24
TiO_2	0.03	0.00	0.04	0.02	0.00	0.00	0.01	0.00	0.00	0.01	0.01
Al_2O_3	21.22	21.40	20.92	21.97	21.91	21.58	21.71	22.06	21.66	21.74	21.53
FeO	31.23	30.61	31.43	29.80	29.16	28.51	29.02	28.52	29.69	29.58	32.27
MnO	0.76	0.62	0.80	0.62	0.63	0.62	0.80	0.72	0.83	0.91	1.75
MgO	5.50	5.67	5.47	6.65	6.75	6.53	6.43	6.43	5.85	5.77	4.41
CaO	3.63	3.11	3.26	3.59	3.38	4.08	4.15	4.10	3.80	3.95	2.22
Na_2O	BDL	BDL	0.04	BDL	0.01	BDL	0.03	0.04	0.02	0.04	0.05
Total	99.42	98.59	99.16	99.98	99.95	99.01	100.09	99.97	99.15	99.81	99.47
Si	2.937	2.966	2.959	2.915	2.973	2.967	2.959	2.971	2.951	2.969	2.975
Ti	0.002	0.000	0.003	0.001	0.000	0.000	0.000	0.000	0.000	0.000	0.000
Al	1.983	2.012	1.962	2.022	2.014	2.003	1.996	2.027	2.018	2.013	2.028
Fe^{3+}	0.079	0.023	0.077	0.062	0.013	0.030	0.045	0.002	0.031	0.018	0.000
Fe^{2+}	1.991	2.019	2.014	1.884	1.889	1.847	1.848	1.857	1.932	1.926	2.160
Mn	0.051	0.042	0.054	0.041	0.042	0.041	0.053	0.048	0.055	0.061	0.118
Mg	0.650	0.674	0.648	0.774	0.785	0.767	0.748	0.747	0.689	0.676	0.525
Ca	0.308	0.265	0.278	0.301	0.282	0.345	0.347	0.342	0.322	0.332	0.190
Na	--	--	0.006	--	0.002	--	0.004	0.005	0.002	0.006	0.007
	8.000	8.000	8.000	7.999	8.000	8.000	8.000	8.000	8.000	8.000	8.003
X_{Fe}	0.75	0.75	0.76	0.71	0.71	0.71	0.71	0.71	0.74	0.74	0.80
Grs	0.10	0.09	0.09	0.10	0.09	0.11	0.12	0.11	0.11	0.11	0.06
Prp	0.22	0.22	0.22	0.26	0.26	0.26	0.25	0.25	0.23	0.23	0.18
Alm	0.66	0.67	0.67	0.63	0.63	0.62	0.62	0.62	0.64	0.64	0.72
Sps	0.02	0.01	0.02	0.01	0.01	0.01	0.02	0.02	0.02	0.02	0.04

Formula calculated on the basis of 8 cations. Fe^{3+} calculated by stoichiometry. $X_{Fe} = Fe^{2+}/(Fe^{2+} + Mg)$. BDL, below detection limit.

Table 3

NB2, NB11 (Melanocratic migmatite)									
#37	#40	#41	#64	#65	#66	#81	#82	#80	#102
mantle	mantle	mantle	mantle	mantle	mantle	mantle	mantle	mantle	mantle
37.32	36.96	37.02	36.64	36.95	37.26	36.06	36.25	36.28	37.08
0.01	0.00	0.00	0.00	0.02	0.00	0.00	0.00	0.01	0.00
21.42	21.41	21.75	21.32	21.09	21.10	21.08	20.82	21.06	21.44
32.69	32.52	32.40	32.19	32.80	32.45	33.24	33.40	33.03	32.54
1.72	1.54	1.55	1.51	1.65	1.56	3.37	3.62	3.54	1.16
4.25	4.48	4.48	4.48	4.57	4.45	3.21	3.06	2.99	5.23
2.28	2.62	2.60	2.85	2.79	2.80	1.75	1.59	1.88	2.22
0.01	0.01	0.03	0.01	BDL	0.05	0.01	0.01	0.02	0.02
99.70	99.53	99.82	99.00	99.87	99.67	98.72	98.74	98.81	99.70
2.981	2.951	2.944	2.940	2.943	2.971	2.937	2.957	2.955	2.944
0.000	0.000	0.000	0.000	0.001	0.000	0.000	0.000	0.000	0.000
2.016	2.015	2.039	2.015	1.979	1.983	2.023	2.002	2.021	2.006
0.002	0.033	0.017	0.045	0.077	0.045	0.040	0.041	0.024	0.050
2.181	2.138	2.138	2.115	2.108	2.119	2.224	2.237	2.225	2.111
0.117	0.104	0.105	0.103	0.111	0.106	0.232	0.250	0.244	0.078
0.506	0.533	0.531	0.535	0.543	0.528	0.390	0.372	0.363	0.619
0.195	0.224	0.221	0.245	0.238	0.240	0.153	0.139	0.164	0.189
0.001	0.001	0.005	0.002	--	0.008	0.001	0.002	0.003	0.004
8.000	8.000	8.000	8.000	8.000	8.000	8.000	8.000	8.000	8.000
0.81	0.80	0.80	0.80	0.80	0.80	0.85	0.86	0.86	0.77
0.07	0.07	0.07	0.08	0.08	0.08	0.05	0.05	0.05	0.06
0.17	0.18	0.18	0.18	0.18	0.18	0.13	0.12	0.12	0.21
0.73	0.71	0.71	0.71	0.70	0.71	0.74	0.75	0.74	0.70
0.04	0.03	0.03	0.03	0.04	0.04	0.08	0.08	0.08	0.03

TABLE 4
Average compositions of white mica included in zircon and, for comparison, from other microstructural positions

sample	NB7		NB7		NB7	NB7		NB2		NB2	
Domain	zircon core (n=5)	s.d.	zircon mantle (n=5)	s.d.	zircon mantle	rock matrix (n=8)	s.d.	zircon core (n=3)	s.d.	zircon mantle (n=17)	s.d.
SiO_2	47.63	0.75	48.23	0.97	47.91	50.13	0.48	46.05	1.78	48.20	0.92
TiO_2	1.16	0.77	1.61	0.61	0.17	0.05	0.07	1.18	0.04	1.41	0.34
Al_2O_3	33.61	1.77	33.53	1.50	39.83	31.40	0.50	34.29	1.51	33.13	0.99
FeO	1.20	0.41	1.07	0.53	0.24	1.14	0.18	1.13	0.04	1.45	0.28
MnO	0.01	0.01	0.03	0.00	BDL	BDL	--	0.01	0.01	0.02	0.02
MgO	1.46	0.33	1.44	0.35	0.13	2.73	0.09	1.04	0.07	1.59	0.31
CaO	0.03	0.03	0.02	0.03	0.81	BDL	--	0.03	0.03	0.02	0.01
Na_2O	0.68	0.13	1.01	0.31	6.17	BDL	--	0.77	0.05	0.59	0.22
K_2O	9.14	0.25	8.56	1.11	0.79	11.49	0.11	9.09	0.36	9.23	0.45
Total	99.49		95.48		96.05	96.94		93.58		95.64	0.95
Si	6.267	0.088	6.282	0.066	6.029	6.544	0.042	6.160	0.029	6.299	0.082
Al[4]	1.733	0.088	1.718	0.066	1.971	1.456	0.042	1.840	0.029	1.701	0.082
Al[6]	3.477	0.171	3.429	0.143	3.936	3.375	0.031	3.566	0.022	3.403	0.091
Ti	0.116	0.076	0.157	0.059	0.016	0.004	0.007	0.118	0.003	0.138	0.033
Fetot	0.132	0.046	0.118	0.060	0.025	0.124	0.022	0.126	0.007	0.159	0.031
Mn	0.001	0.001	0.004	0.000	--	--	--	0.001	0.001	0.002	0.003
Mg	0.287	0.067	0.281	0.072	0.024	0.532	0.018	0.208	0.014	0.310	0.060
Ca	0.005	0.005	0.003	0.004	0.110	--	--	0.004	0.004	0.002	0.002
Na	0.174	0.034	0.253	0.075	1.507	--	--	0.201	0.022	0.150	0.057
K	1.534	0.039	1.424	0.206	0.127	1.914	0.019	1.554	0.125	1.538	0.075
K/(K+Na)	0.90		0.85		0.08			0.89		0.91	
X_{Fe}	0.31		0.28		0.51			0.38		0.34	

Formula recalculated on the basis of 42 valencies without interlayer cation. All iron as Fe^{2+}. $X_{Fe} = Fe_{tot}/(Fe_{tot} + Mg)$

Table 4

NB2		NB2		NB11		NB11		NB16		NB16	NB16
in garnet (n=7)	s.d.	rock matrix (n=7)	s.d.	zircon core (n=5)	s.d.	zircon mantle (n=3)	s.d.	zircon core (n=6)	s.d.	zircon mantle	zircon mantle
46.78	0.27	45.79	0.23	47.96	0.53	48.39	0.73	46.21	1.03	48.97	45.20
1.08	0.20	1.14	0.38	1.59	0.13	1.06	0.58	1.17	0.39	0.11	0.07
33.76	0.57	35.14	0.88	31.95	1.29	33.46	1.19	32.47	0.86	29.56	35.08
1.57	0.16	1.23	0.10	1.78	0.46	1.57	0.22	2.77	0.42	3.17	2.48
0.01	0.01	BDL	--	BDL	--	BDL	--	BDL	--	0.01	BDL
1.12	0.14	0.71	0.21	1.99	0.31	1.69	0.41	1.36	0.15	1.87	0.53
0.01	0.01	0.01	0.01	0.02	0.02	0.03	0.02	0.01	0.02	0.06	0.27
1.06	0.07	1.21	0.11	0.44	0.17	0.51	0.06	0.50	0.22	0.45	1.56
9.80	0.11	9.64	0.10	9.52	0.11	9.33	0.51	9.73	0.51	9.58	8.41
95.19		94.88		95.27	0.49	96.05		98.67		93.78	93.59
6.220	0.024	6.105	0.037	6.325	0.083	6.297	0.072	6.223	0.070	6.600	6.109
1.780	0.024	1.895	0.037	1.675	0.083	1.703	0.072	1.777	0.070	1.400	1.891
3.520	0.052	3.627	0.092	3.289	0.093	3.430	0.143	3.378	0.058	3.295	3.697
0.110	0.021	0.114	0.038	0.158	0.013	0.104	0.056	0.119	0.037	0.011	0.007
0.180	0.017	0.138	0.011	0.197	0.052	0.171	0.023	0.312	0.050	0.357	0.280
0.000	0.001	--	--	--	--	--	--	--	--	0.001	--
0.220	0.028	0.142	0.041	0.391	0.063	0.327	0.078	0.272	0.027	0.376	0.106
0.000	0.001	0.001	0.001	0.003	0.003	0.004	0.002	0.002	0.003	0.009	0.039
0.270	0.018	0.312	0.027	0.114	0.044	0.129	0.014	0.131	0.057	0.118	0.410
1.660	0.019	1.640	0.018	1.602	0.025	1.550	0.103	1.673	0.109	1.647	1.451
0.86		0.84		0.93		0.92		0.93		0.93	0.78
0.44		0.50		0.33		0.35		0.53		0.49	0.73

TABLE 5

Composition of biotite included in zircon mantle and, for comparison, from other microstructural positions

sample	NB7	NB7	NB7	NB7		NB2	NB2	NB11		NB11	NB11	NB11		NB11		NB16	
Domain	zircon core	zircon mantle	zircon mantle	rock matrix (n=8)	s.d.	zircon core	zircon mantle	zircon core (n=7)	s.d.	zircon mantle	zircon mantle	in garnet (n=10)	s.d.	rock matrix (n=12)	s.d.	zircon core (n=3)	s.d.
SiO_2	34.40	36.95	37.65	37.33	0.43	35.02	35.62	35.38	1.30	35.68	33.83	35.54	0.44	34.96	0.13	36.01	0.98
TiO_2	1.38	2.37	3.03	2.60	0.36	3.28	1.58	2.62	0.95	3.32	0.35	2.25	0.38	2.39	0.22	2.00	0.51
Al_2O_3	19.53	18.29	17.84	18.13	0.60	18.76	19.71	17.97	0.80	15.73	18.30	19.14	0.19	19.05	0.25	18.29	0.44
FeO	21.91	12.92	13.92	10.96	0.52	20.29	18.47	18.12	0.96	17.20	19.69	19.24	0.90	20.35	0.37	13.61	0.85
MnO	0.12	0.03	BDL	0.02	0.03	0.00	0.03	0.05	0.04	BDL	0.08	0.01	0.02	0.01	0.01	0.03	0.03
MgO	9.02	14.29	14.59	16.71	0.53	9.35	11.23	11.13	0.94	11.23	12.54	10.54	1.03	9.50	0.22	15.41	2.84
CaO	0.04	BDL	0.03	0.03	0.01	0.08	0.12	0.03	0.03	0.02	0.04	0.01	0.02	0.03	0.04	0.00	0.00
Na_2O	0.08	0.27	0.25	0.16	0.07	0.11	0.48	0.09	0.07	0.16	0.02	0.31	0.04	0.31	0.05	0.26	0.12
K_2O	8.56	8.98	8.99	9.75	0.25	9.19	7.49	9.05	0.94	9.03	8.11	9.02	0.29	8.90	0.21	8.70	0.67
Total	95.06	94.10	96.30	95.70		96.09	94.73	94.44		92.37	92.96	96.05		95.51		94.33	1.01
Si	2.649	2.748	2.746	2.716	0.027	2.654	2.683	2.699	0.062	2.779	2.639	2.674	0.020	2.662	0.010	2.684	0.063
Al[4]	1.351	1.252	1.254	1.284	0.027	1.346	1.317	1.301	0.062	1.221	1.361	1.326	0.020	1.338	0.010	1.316	0.063
Ti	0.080	0.132	0.166	0.143	0.020	0.187	0.089	0.150	0.054	0.195	0.021	0.127	0.022	0.137	0.013	0.112	0.028
Al[6]	0.421	0.351	0.280	0.271	0.037	0.330	0.432	0.316	0.061	0.223	0.322	0.371	0.011	0.372	0.014	0.291	0.095
Fe_{tot}	1.411	0.803	0.849	0.667	0.031	1.286	1.163	1.157	0.069	1.120	1.285	1.210	0.062	1.296	0.023	0.849	0.049
Mn	0.008	0.002	--	0.001	0.002	0.000	0.002	0.003	0.002	--	0.006	0.001	0.001	0.000	0.001	0.002	0.002
Mg	1.035	1.584	1.587	1.813	0.054	1.057	1.261	1.266	0.115	1.304	1.458	1.181	0.108	1.079	0.023	1.713	0.319
Ca	0.004	--	0.002	0.002	0.001	0.007	0.010	0.002	0.003	0.002	0.003	0.001	0.002	0.003	0.003	0.000	0.000
Na	0.012	0.038	0.035	0.022	0.010	0.017	0.071	0.013	0.011	0.024	0.003	0.045	0.005	0.046	0.008	0.038	0.017
K	0.841	0.852	0.837	0.905	0.024	0.889	0.719	0.881	0.087	0.898	0.807	0.866	0.032	0.865	0.019	0.828	0.063
X_{Fe}	0.58	0.34	0.35	0.27	0.01	0.55	0.48	0.48	0.02	0.46	0.47	0.51	0.03	0.55	0.01	0.33	0.05

Formula recalculated on the basis of 21 valencies without interlayer cation. All iron as Fe^{2+}. $X_{Fe} = Fe_{tot}/(Fe_{tot} + Mg)$

TABLE 2
Semiquantitative analyses of "glass" included in zircon

	Grt-Ky gneiss (n=5)		Mela-migmatites (n=13)		Leuco-migmatite (n=3)		Experimental glass*	
	min	max	min	max	min	max	min	max
SiO_2	70.18	74.67	70.32	74.98	72.96	75.27	73.20	75.60
TiO_2	0.00	0.03	0.00	0.99	0.01	0.02	0.03	0.29
Al_2O_3	12.52	16.80	12.09	19.49	11.81	12.70	14.95	16.36
FeO	0.00	0.71	0.00	0.56	0.03	0.12	0.70	1.08
MnO	0.00	0.05	0.00	0.03	0.00	0.04	0.02	0.07
MgO	0.01	0.08	0.00	0.22	0.04	0.08	0.17	0.41
CaO	0.81	2.99	0.02	2.51	0.55	2.76	0.42	1.52
Na_2O	0.81	7.54	0.16	5.98	1.23	3.31	3.07	6.67
K_2O	0.67	3.69	1.91	7.73	1.87	2.13	1.71	5.19
A/(CNK)	0.94	2.66	1.10	3.61	1.31	1.61	1.03	1.41

* from Patino-Douce and Harris, 1998

zircon mantle. Biotite in zircon from melanocratic migmatites displays X_{Fe} and Si ranging between 0.46-0.55 and 2.58-2.78 apfu, respectively. Biotite included in garnet and from the rock matrix shows narrower compositional variations with respect to the biotite included in zircon. In the leucocratic migmatite, only three biotites were found to be included in the zircon core: these biotites form a rough positive trend from X_{Fe} = 0.28, Si = 2.61 apfu to X_{Fe} = 0.38, Si = 2.74 apfu.

Plagioclase solely occurring in zircon cores is albite or oligoclase in all studied samples. Only one grain of *alkali-feldspar* in zircon from the leucocratic migmatite was found to be part of a composite inclusion together with former melt. The small size of this feldspar grain did permit a semiquantitative analysis only.

P-T PSEUDOSECTION

The presence of abundant rounded inclusions interpreted as former inclusions of peraluminous melt indicates that zircon interacted with a felsic melt that partially dissolved the (probably mainly detrital) cores. As a result, the inherited cores show curvilinear and embayed shapes. This melt is most likely related to the last partial melting that the UZ crust underwent ~ 330 Ma ago, as determined by Sm-Nd age dating of migmatites (Tumiati *et al.*, 2003). An important feature is that the former melt inclusions occur in the zircon mantle that also contains potassic white-mica and biotite. This implies that during anatexis the *P-T* conditions were compatible with the presence of two micas and silicate liquid. In order to quantify these physical conditions attained during the coexistence of micas and silicate liquid, we calculated an isochemical phase diagram, i.e. a *P-T* pseudosection, to represent quantitatively the *P-T* field(s) related to biotite-white-mica-melt-bearing assemblages.

The *P-T* pseudosection (for calculation method see Braga *et al.*, 2007) of Fig. 8 has been obtained using the updated (May 2008) version of PERPLE_X (Connolly, 1990) in the *P-T* frame 5-30 kbar and 500-1000 °C. This frame includes all the previously inferred *P-T* evolutions of the UZ gneisses and migmatites (see above). The solid solution phases (with sources of thermodynamic mixing models) and the equation of state of water are reported in the Appendix. As input composition we considered the Post Archean Average Shales (PAAS) reported by Taylor and McLennan (1985). These shales

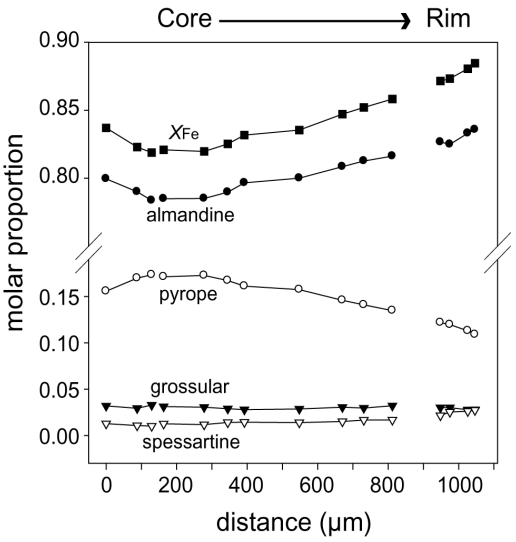

Fig. 6 – Core-rim zoning of a coarse-grained garnet in the matrix of a melanocratic migmatite.

show major and trace element compositions similar to the less migmatized UZ crust (Tumiati *et al.*, 2007), suggesting that the PAAS may represent the composition of the protolith of the UZ crust. The shale major-element composition was simplified to the Na_2O-CaO-K_2O-FeO-MgO-Al_2O_3-SiO_2-TiO_2-H_2O chemical system by adding MnO, present in minor amounts in garnet, to the total FeO and by ignoring P_2O_5 that is mainly present in apatite and monazite. The H_2O content of the rock has been set to 1.1 wt%, which represents the average amount of H_2O bounded to micas in pelitic rocks (see, e.g., Clemens and Vielzeuf, 1987). Another simplification regards the Fe^{3+} content of the bulk rock. Major minerals of metapelites such as biotite and, to a lesser extent, garnet incorporate small amounts of ferric iron. However, without a complete chemical analysis, including H^+, F^- and Cl^-, the ferric iron estimation in biotite is fraught with large uncertainties (see Braga *et al.*, 2006). Therefore, we decided to consider the whole iron content as FeO.

The above simplifications can result only in approximations of the true composition of the protolith of the UZ crust. This is particularly true in regard of the H_2O content considered in the input bulk composition. A higher H_2O content would shift the onset of partial melting to lower *T* and would likely enlarge the *P-T* field where white mica + biotite + melt coexist. Previous petrological studies favour fluid-present conditions for the metamorphic evolution of the UZ crust (Godard *et al.*, 1996; Hauzenberger *et al.*, 1996). However, water contents of a rock change with metamorphic grade and it is likely that fluid-deficient conditions prevail in the lower crust (Clemens and Vielzeuf, 1987). Accordingly, the selected H_2O content allows to calculate, for the UZ crust, high-grade metamorphism and partial melting in a fluid-absent system, which is the model already proposed by Benciolini and Poli (1993).

The assemblage biotite + white-mica + kyanite + melt is stable along a narrow bivariant field ranging between ~ 750-800 °C and 8.5-12.5 kbar (dashed ellipsoid in Fig. 8). The upper *P* limit is defined by the disappearance of biotite whereas the upper *T* limit is marked by the exhaustion of white-mica during the partial melting reactions. The pseudosection also predicts the presence of plagioclase and alkali-feldspar in the marked field. However, these phases are not commonly preserved as inclusions in the zircon mantle. The (apparent) lack of feldspar inclusions (although one K-feldspar inclusion has been observed in zircon from leuco-migmatite NB16) may have several possible causes: (a) the number of inclusions investigated in this study was limited; (b) the bulk composition chosen is richer in alkalis than in the studied rock samples with the results that feldspars occur over a wider *P-T* range than relevant to our samples; (c) lack of a reliable activity model for feldspar at high-pressure (O'Brien, 2008) and thus the thermodynamic calculations overestimate the modal abundances of these two phases, (d) the inclusion process of minerals in zircon is hardly understood yet and, thus, it might be likely that the abundance of minerals in zircon does not represent the modal composition of a rock when the inclusion process is running. Zircon from the garnet-kyanite gneiss and melanocratic migmatite do not contain inclusions of kyanite. The kyanite modal abundance modeled by the pseudosection at 12 kbar and 770 °C (i.e., just below the solidus conditions) is less than 4%. Such a low modal content may hamper the possibilities to find kyanite included in zircon.

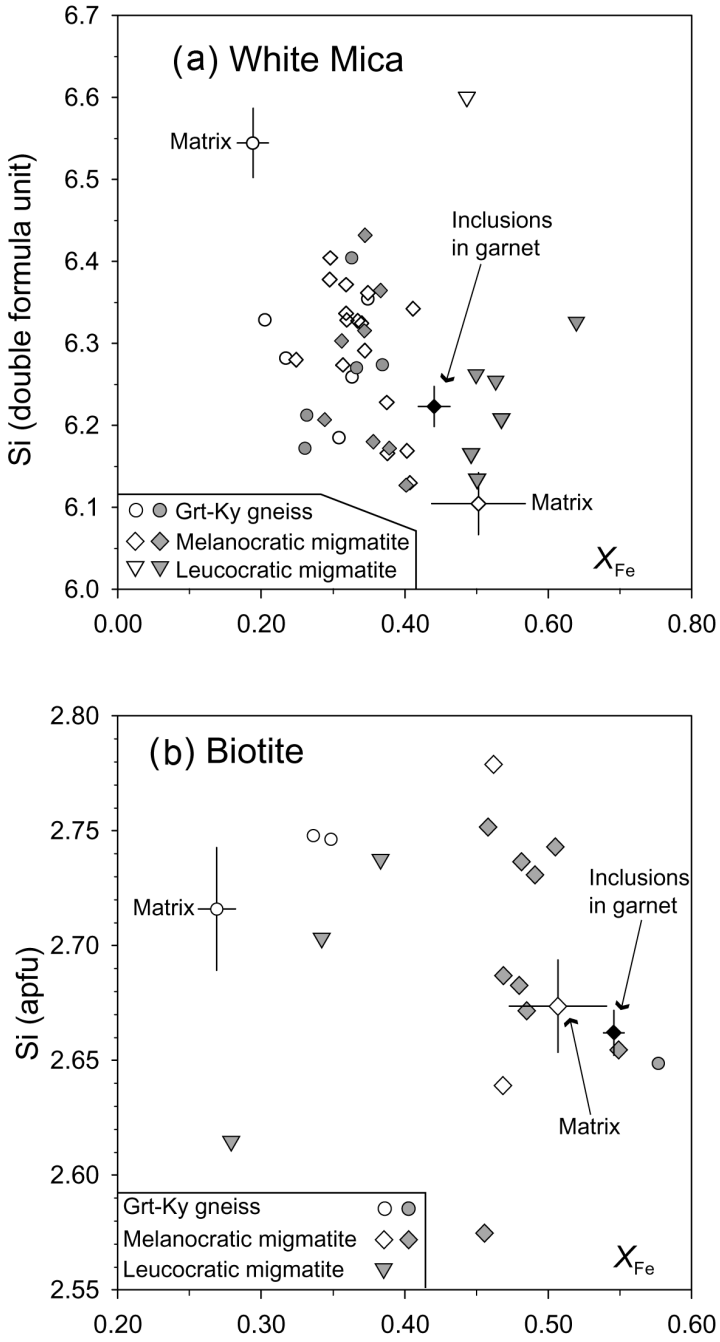

Fig. 7 – Relationship between Si and X_{Fe} of enclosed white-mica (A) and biotite (B) and comparison with micas from different microstructural positions. Closed and open symbols refer to minerals included in zircon core and mantle, respectively. Bars refer to compositional ranges.

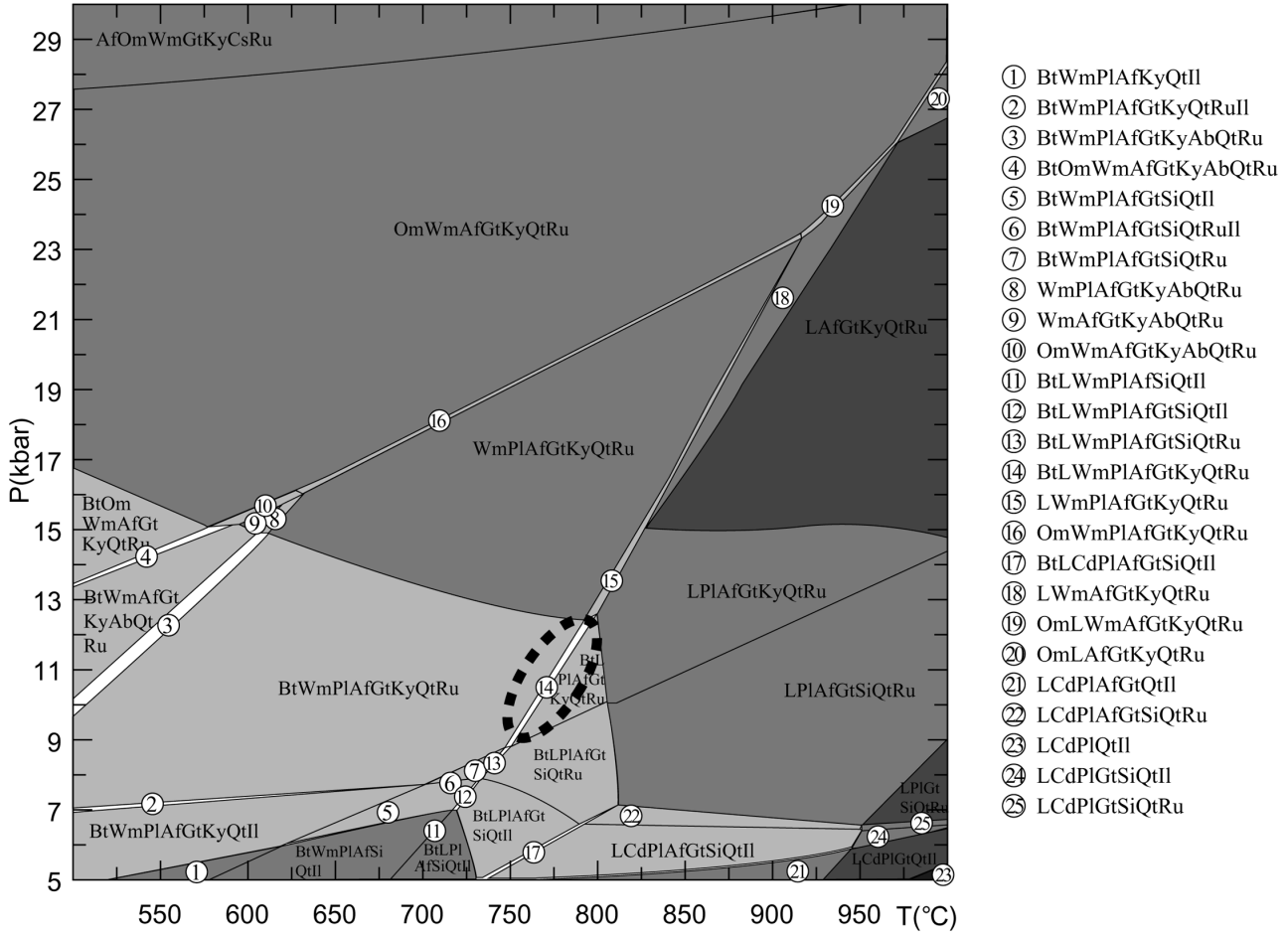

① BtWmPlAfKyQtIl
② BtWmPlAfGtKyQtRuIl
③ BtWmPlAfGtKyAbQtRu
④ BtOmWmAfGtKyAbQtRu
⑤ BtWmPlAfGtSiQtIl
⑥ BtWmPlAfGtSiQtRuIl
⑦ BtWmPlAfGtSiQtRu
⑧ WmPlAfGtKyAbQtRu
⑨ WmAfGtKyAbQtRu
⑩ OmWmAfGtKyAbQtRu
⑪ BtLWmPlAfSiQtIl
⑫ BtLWmPlAfGtSiQtIl
⑬ BtLWmPlAfGtSiQtRu
⑭ BtLWmPlAfGtKyQtRu
⑮ LWmPlAfGtKyQtRu
⑯ OmWmPlAfGtKyQtRu
⑰ BtLCdPlAfGtSiQtIl
⑱ LWmAfGtKyQtRu
⑲ OmLWmAfGtKyQtRu
⑳ OmLAfGtKyQtRu
㉑ LCdPlAfGtQtIl
㉒ LCdPlAfGtSiQtRu
㉓ LCdPlQtIl
㉔ LCdPlGtSiQtIl
㉕ LCdPlGtSiQtRu

Fig. 8 – *P–T* pseudosection for the system Na_2O-CaO-K_2O-FeO-MgO-Al_2O_3-SiO_2-TiO_2-H_2O. The input composition, which is the Post Archean Average Shales of Taylor and McLennan (1985), is (in wt%): Na_2O = 1.22, CaO = 1.32, K_2O = 3.75, total FeO = 6.59, MgO = 2.23, Al_2O_3 = 19.15, SiO_2 = 63.63, H_2O = 1.11. Very narrow bivariant fields were omitted to improve the diagram presentation. Divariant fields are unshaded; grey intensity increases with the variance increasing. Mineral abbreviations: Bt, biotite; Wm, potassic white-mica; Gt, garnet; Ky, kyanite; Si, sillimanite; Pl, plagioclase; Af, alkali-feldspar; L, melt; Qt, quartz; Ru, rutile; Il, ilmenite; Ab, albite; Cd, cordierite, Om, omphacite; Cs, coesite. The dashed ellipsoid outlines the *P-T* region where micas, kyanite, and melt coexist.

Discussion

The message from the included phases

Zircon separated from representative rocks of the UZ crust reveals a variety of inclusions in different zircon domains. The Si-rich and peraluminous composition (Table 2) of the former melt inclusions, which occur at the boundary between zircon core and mantle or rarely within cores with igneous structure (planar oscillatory zoning), reflects partial melting of an Al-rich metasedimentary source. The obvious candidate of this source is the UZ garnet-kyanite gneiss, which is very likely the protolith of the UZ migmatites (Godard *et al.*, 1996). The above melt inclusions are, thus, a further witness of the Carboniferous anatectic event recorded by the UZ crust.

Biotite and potassic white-mica inclusions are present in the core and mantle domains of zircon, suggesting that the UZ crust underwent a metamorphic evolution within the stability field of these minerals. Assemblages with biotite and potassic white-mica are only stable if the corresponding metamorphic *P-T* path is characterized by loops that do not exceed 17 kbar (at low *T*) or 13 kbar (at high *T*) in metapelitic compositions similar to that of the PAAS (Fig. 8). It is interesting to note that biotite may be present over a *P-T* range that is commonly recorded by crustal rocks involved in a collisional process. This poses the problem to identify biotite grains related to the prograde or retrograde portion of the *P-T* path. In the UZ, for instance, biotite has been generally considered as a retrograde, low-*P* product. In metapelitic rocks, one possible criterion to distinguish H*P* from L*P* biotite is to monitor its Si content. Experiments on model crustal compositions (e.g., Hermann, 2002) and observations on metapelitic rocks (e.g., Miyashiro and Shido, 1985) have shown that Si content in biotite increases with increasing pressure, thus paralleling the well-known celadonite substitution in phengitic mica (Massonne and Schreyer, 1987). In our study, a few included biotite in the zircon mantle show higher Si content (~ 2.75 apfu) than matrix biotite and this chemical feature along with the coexistence of biotite and former melt inclusions support the notion that at least part of the included biotite equilibrated at peak pressure metamorphic conditions. According to experimental work (Hermann, 2002), biotite with 2.9 apfu should be typical for biotite equilibrated close to 20 kbar at T = 750 – 800 °C. In our study, the Si content of biotite does not exceed 2.8 a.p.f.u., which is in agreement with significantly lower pressures than 20 kbar as also predicted by the *P-T* pseudosection results (see also Braga *et al.*, 2007).

Garnet included in zircon separated from the melanocratic migmatites is richer in Ca than the matrix garnet (Fig. 6). In the *P-T* range considered in this study, garnet X_{Ca} isopleths have a positive slope (Indares, 1995; Spear and Khon, 1996; Indares *et al.*, 2008) and a decrease in X_{Ca} may be due either to a decrease in P or to an increase in T, or to a combination of these two factors. As a consequence, the observed X_{Ca} variation between included and matrix garnet can be related to a prograde portion of a *P-T* path characterized by the lack of *P* increase. We propose that a (near) isothermal heating would represent a favourable scenario to explain the omnipresence of the low-medium *P* assemblage (garnet + potassic white-mica + biotite) and mineral compositions (relatively low Si contents in potassic white-mica and biotite).

Another hint at about the early metamorphic evolution of the UZ crust is the presence of medium grade minerals in the core of zircon from the garnet-kyanite gneiss such as chlorite, paragonite, zoisite/clinozoisite and staurolite. All these minerals are also observed in large kyanite porphyroblast from the UZ gneisses and belong to a prograde amphibolite-facies stage (Braga *et al.*, 2007).

Geodynamic insights

The timing of the migmatization event during the UZ metamorphic evolution is controversial. According to Godard *et al.* (1996), migmatization occurred along the retrograde path during exhumation of the UZ basement whereas Hauzenberger *et al.* (1996) proposed that the migmatites formed during the prograde metamorphic evolution of the UZ crust, at peak-*P* and fluid-present conditions. On the other hand, Tumiati *et al.* (2003) considers that partial melting of the UZ gneisses occurred at peak metamorphic conditions (~ 27 kbar, 850 °C). Our results indicate, however, that partial melting is related to peak

metamorphic temperatures at pressures below 13 kbar. The peak pressure (≤ 15 kbar representing the maximum pressure stability of biotite in albite-free assemblages) was reached prior to the partial melting event. As proposed by Braga *et al.* (2007), the lithospheric delamination model, that implies the influx of astenospheric hot mantle, replacing dense lower crust after the Variscan collision may explain concomitant pressure release and heating. A crustal delamination model is also proposed by Perchuk *et al.* (2007) for the UZ. Conversely, the residence of portions of the UZ crust at mantle depths of about 90 km (Tumiati *et al.*, 2003; Ranalli *et al.*, 2005) is not supported by mineralogical evidence.

Conclusions

The mineralogy of the inclusions in the mantle of zircon, separated from a garnet-kyanite gneiss and three migmatites, along with calculations of a *P-T* pseudosection indicate that the peak metamorphic evolution and concomitant anatexis of the UZ crust occurred between 750-800 °C and 8.5-12.5 kbar. The prograde (i.e. *T* increase) portion of the metamorphic path is likely characterized by lack of pressure increase. Very high-*P* conditions (27 kbar at 850 °C, see Tumiati *et al.,* 2003) require the presence of corresponding indicator minerals, such as Na-pyroxene or high-Si phengite, at least as inclusion in zircon or garnet. However, no such indicator mineral has been observed. Instead, low-medium pressure minerals such as biotite and relatively low-Si white-mica were preserved. The presence of biotite included in zircon mantle and widespread in the rock matrix is due to its large *P-T* stability up to 13-15 kbar and more than 800 °C, as shown here by thermodynamic calculations. If the metamorphic evolution of metapelitic crust remains within this *P-T* frame, which is common in continent-continent collision zones, then peak (and even prograde) biotite might be preserved in zircon.

Acknowledgement

We thank Concezio Fagnano (Dipartimento di Biochimica "Giovanni Moruzzi", Università di Bologna) for micro-Raman spectra and Thomas Theye (Universität Stuttgart) for support during the microprobe work. Dieter Dettmar (Ruhr-Universität Bochum) prepared the polished zircon specimens. The manuscript benefited from useful comments by R. Compagnoni. L. Morbidelli is thanked for the editorial handling. The MIUR-Cofin, Marco Polo and Vigoni funding schemes supported the stay of R.B. in Stuttgart.

APPENDIX

Thermodynamic models of the minerals (with the PERPLE_X code) chosen for the pseudosection calculations are:

Garnet, Gt(HP), (Holland and Powell, 1998).

Biotite, TiBio(HP), (Powell and Holland, 1999);

Paragonite, MuPa, (Chatterjee and Froese, 1975)

Phengite, Pheng(HP), http://www.esc.cam.ac.uk/astaff/holland/ds5/muscovites/mu.html;

Plagioclase, Pl(h), (Newton *et al.*, 1980);

Alkali feldspar, San, (Waldbaum and Thompson, 1969);

Silicate liquid, melt(HP), (Holland and Powell, 2001; White *et al.*, 2001);

Omphacite, Omph(HP), (Holland and Powell, 1996);

Cordierite, hCrd, (Holland and Powell, 1998)

Staurolite, St(HP), (Holland and Powell, 1998).

The equation of state for H_2O is the CORK (Holland and Powell, 1991; Holland and Powell, 1998).

References

Bargossi G.M., Bondi M., Mordenti A. and Morten L. (2003) - *The abundances of 55 elements and petrovolumetric models of the crust in the Non and Ulten Valleys (Site 3)*. Scritti e documenti dell'Accademia Nazionale delle Scienze detta dei XL, **32**, 163-196.

Benciolini N. and Poli S. (1993) - *The lower continental crust in the Tonale nappe (Upper Austroalpine, Ultental): new petrological constraints.* Terra Abstract, **5**, 398

Bousquet R. (2008) - *Metamorphic heterogeneities within a single HP unit: Overprint effect or metamorphic mix?* Lithos, **103**, 46-69.

Braga R., Massonne H.-J. and Morten L. (2007) - *An early metamorphic stage for the Variscan*

Ulten Zone gneiss (NE Italy): evidence from mineral inclusions in kyanite. Mineral. Mag., **71**, 691-702.

Braga R., Morten L. and Zanetti A. (2006) - *Origin of a mica megacryst in an alkaline dyke from the Veneto Volcanic Province, Italy*. Eur. J. Mineral., **18**, 223-231.

Chatterjee N. D. and Froese E. (1975) - A thermodynamic study of the pseudobinary join muscovite-paragonite in the system $KAlSi_3O_8$-$NaAlSi_3O_8$-Al_2O_3-SiO_2-H_2O. Am. Mineral., **60**, 985-993.

Chopin C. and Sobolev N.V. (1995) - *Principal mineralogic indicators of UHP in crustal rocks*. In R.G. Coleman and X. Wang (Eds.), Ultrahigh-Pressure Metamorphism, Cambridge University Press, pp. 96-133.

Clemens J.D. and Vielzeuf D. (1987) - *Constraints on melting and magma production in the crust*. Earth Planet. Sci. Lett., **86**, 287-306.

Connolly J.A.D. (1990) - *Multivariable phase diagrams: an algorithm based on generalized thermodynamics*. Am. J. Sci., **290**, 666-718.

Del Moro A., Martin S. and Prosser G. (1993) - Cooling ages from the migmatite-granulite complex of the Autroalpine Ulten Zone (Eastern Alps). Terra Abstract, **5**, 8.

Del Moro A., Martin S. and Prosser G. (1999) - Migmatites of the Ulten Zone (NE Italy), a record of melt transfer in deep crust. J. Petrol., **40**, 1803-1826.

Godard G., Martin S., Prosser G., Kienast J.R. and Morten L. (1996) - *Variscan migmatites, eclogites and garnet-peridotites of the Ulten zone, Eastern Austroalpine system*. Tectonophysics, **259**, 313-341.

Hauzenberger C.A., Höller W. and Hoinkes G. (1996) - *Transition from eclogite to amphibolite-facies metamorphism in the Australpine Ulten Zone*. Mineral. Petrol., **58**, 111-130.

Hauzenberger C.A., Höller W., Hoinkes G., Klötzli U. and Thöni M. (1993) - Metamorphic evolution of the Austroalpine basement in the Nonsberg area, Ultental (Val d'Ultimo), southern Tyrol. Terra Abstract, **4**, 13.

Hermann J. (2002) - *Experimental constraints on phase relations in subducted continental crust*. Contrib. Mineral. Petrol., **143**, 219-235.

Holland T.J.B. and Powell R. (1991) - *A compensated-Redlich-Kwong (CORK) equation for volumes and fugacities of CO_2 and H_2O in the range 1 bar to 50 kbar and 100-1600°C*. Contrib. Mineral. Petrol., **109**, 265-273.

Holland T. and Powell R. (1996) - *Thermodynamics of order-disorder in minerals: II. Symmetric formalism applied to solid solutions*. Am. Mineral., **81**, 1425-1437.

Holland T.J.B. and Powell R. (1998) - *An internally consistent thermodynamic data set for phases of petrological interest*. J. Metam. Geol., **16**, 309-343.

Holland T. and Powell R. (2001) - *Calculation of phase relations involving haplogranitic melts using an internally consistent thermodynamic dataset*. J. Petrol., **42**, 673-683.

Indares A. (1995) - *Metamorphic interpretation of high-pressure-temperature metapelites with preserved growth zoning in garnet, eastern Grenville Province, Canadian Shield*. J. Metam. Geol., **13**, 475-486.

Indares A., White R.W. and Powell R. (2008) - *Phase equilibria modelling of kyanite-bearing anatectic paragneisses from the central Grenville Province*. J. Metam. Geol., **26**, 815-836.

Katayama I., Zayachkovsky A.A. and Maruyama S. (2000) - *Prograde pressure-temperature records from inclusions in zircons from ultrahigh-pressure-high-pressure rocks of the Kokchetav Massif, northern Kazakhstan*. The Island Arc, **9**, 417-427.

Liu J., Ye K., Maruyama S., Cong B. and Fan H. (2001) - *Mineral Inclusions in zircon from gneisses in the ultrahigh-pressure zone of the Dabie Mountains, China*. J. Geol., **109**, 523-535.

Massonne H.-J. and Schreyer W. (1987) - *Phengite geobarometry based on the limiting assemblage with K-feldspar, phlogopite and quartz*. Contrib. Mineral. Petrol., **96**, 212-224.

Massonne H.-J. and Nasdala L. (2003) - *Characterization of an early metamorphic stage through inclusions in zircon of a diamondiferous quartzofeldspathic rock from the Erzgebirge, Germany.* Am. Mineral., **88**, 883-889.

Miyashiro A. and Shido F. (1985) - *Tschermak substitution in low- and middle-grade pelitic schists.* J. Petrol., **26**, 449-487.

Newton R.c., Charlu T.v. And Kleppa O.j. (1980) - *Thermochemistry of the high structural state plagioclases*. Geochim. Cosmochim. Acta, **44**, 933-941.

Nimis P. and Morten L. (2000) - *P-T evolution of 'crustal' garnet peridotites and included pyroxenites from Nonsberg area (upper Austroalpine), NE Italy: from the wedge to the slab*. J. Geodyn., **30**, 93-115.

Obata M. and Morten L. (1987) - *Transformation of spinel lherzolite to garnet lherzolite in ultramafic*

lenses of the Austridic crystalline complex, Northern Italy. J. Petrol., **28**, 599-623.

O'Brien P.J. (2008) - *Challenges in high-pressure granulite metamorphism in the era of pseudosections: reaction textures, compositional zoning and tectonic interpretation with examples from the Bohemian Massif*. J. Metam. Geol., **26**, 235-251.

Parkinson C.D. and Katayama I. (1999) - *Present-day ultrahigh-pressure conditions of coesite inclusions in zircon and garnet: Evidence from laser Raman microspectroscopy*. Geology, **27**, 979-982.

Patiño Douce A.E. (1999) - *What do experiments tell us about the relative contributions of crust and mantle to the origin of granitic magmas?* In A. Castro, C. Fernandez and J.L. Vigneresse (Eds.), Understanding granites: integrating new and classical techniques. Geol. Soc., **168**, pp. 55-75.

Patiño Douce A.E. and Harris N. (1998) - *Experimental constraints on Himalayan anatexis*. J. Petrol., **39**, 689-710.

Perchuk L.L., Gerya T.V., Parfenova O.V. and Podgornova S.T. (2007) - *Metamorphic Rocks of the Samerberg Complex, Eastern Alps: 2. P–T Paths and the Problem of a Geodynamic Model*. Petrology, **15**, 397-415.

Powell R. and Holland T. (1999) - *Relating formulations of the thermodynamics of mineral solid solutions: Activity modeling of pyroxenes, amphiboles, and micas*. Am. Mineral., **84**, 1-14.

Ranalli G., Martin S. and Mahatsente R. (2005) - *Continental subduction and exhumation: an example from the Ulten Unit, Tonale Nappe, Eastern Austroalpine*. In D. Gapais, J.-P. Brun and P.R. Cobbold (Eds.), Deformation Mechanisms, Rheology and Tectonics: from Minerals to the Lithosphere., pp. 159-174.

Sobolev N.V., Shatsky V., Vavilov M.A. and Goryainov S.V. (1991) - *Coesite inclusion in zircon from diamond-containing gneisses of Kokchetav Massif - 1st find of coesite in metamorphic rocks in the USSR*. Doklady Akademii Nauk SSSR, **321**, 184-188.

Spear F.S. and Kohn M.J. (1996) - Trace element zoning in garnet as a monitor of crustal melting. Geology, 24, 1099-1102.

Tabata H., Yamauchi K., Maruyama S. and Liou J.G. (1998) - *Tracing the extent of a UHP metamorphic terrane: Mineral-inclusion study of zircons in gneiss from the Dabieshan*. In B. Hacker and J. G. Liou (Eds.), When Continents Collide: Geodynamics and Geochemistry of Ultrahigh-pressure Rocks, Kluwer Academic Publishers, pp. 261-273.

Taylor S.R. and Mclennan S.M. (1985) The continental crust: its composition and evolution., pp. 307. Blackwell Scientific.

Thöni M. (1981) - *Degree and evolution of the alpine metamorphsim in the Austroalpine unit W of the Hohe Tauern in the light of K/Ar and Rb/Sr age determinations on micas*. Jahrbuch der Geologischen Bundesanstalt, **124**, 111-174.

Tumiati S., Godard G., Martin S., Klotzli U. and Monticelli D. (2007) - *Fluid-controlled crustal metasomatism within a high-pressure subducted mélange (Mt. Hochwart, Eastern Italian Alps)*. Lithos, **94**, 148-167.

Tumiati S., Thoni M., Nimis P., Martin S. and Mair V. (2003) - *Mantle-crust interactions during Variscan subduction in the Eastern Alps (Nonsberg-Ulten zone): geochronology and new petrological constraints*. Earth Planet. Sci. Lett., **210**, 509-526.

Waldbaum D.R. and Thompson J.B.J. (1969) - *Mixing properties of sanidine crystalline solutions: IV. Phase diagrams from equations of state*. Am. Mineral., **54**, 1274-1298.

White R.W., Powell R. and Holland T.J.B. (2001) - *Calculation of partial melting equilibria in the system Na_2O-CaO-K_2O-FeO-MgO-Al_2O_3-SiO_2-H_2O (NCKFMASH)*. J. Metam. Geol., **19**, 139-153.

Willner A.P., Krohe A. and Maresch W.V. (2000) - *Interrelated P-T-t-d paths in the Variscan Erzgebirge dome (Saxony, Germany): Constraints on the rapid exhumation of high-pressure rocks from the root zone of a collisional orogen.* Int. Geol. Rev., **42**, 64-85.

Ye K., Yao Y., Katayama I., Cong B., Wang Q. and Maruyama S. (2000) - *Large areal extent of ultrahigh-pressure metamorphism in the Sulu ultrahigh-pressure terrane of East China: new implications from coesite and omphacite inclusions in zircon of granitic gneiss*. Lithos, **52**, 157-164.

Young D.J., Hacker B.R., Andersen T.B. and Corfu F. (2007) - *Prograde amphibolite facies to ultrahigh-pressure transition along Nordfjord, western Norway: Implications for exhumation tectonics*. Tectonics, **26**, TC1007.